EXCITATION SIGNAL PROCESSING TIMES IN *HALOBACTERIUM HALOBIUM* PHOTOTAXIS

STEVEN A. SUNDBERG,* MAQSUDUL ALAM,‡ AND JOHN L. SPUDICH*
**Department of Anatomy and Structural Biology, and Department of Physiology and Biophysics, Albert Einstein College of Medicine, Bronx, New York 10461; and ‡Biochemistry and Biophysics Program, Washington State University, Pullman, Washington 99164*

ABSTRACT Phototaxis responses of *Halobacterium halobium* were monitored with a computerized cell-tracking system coupled to an electronic shutter controlling delivery of photostimuli. Automated analysis of rates of change in direction and linear speeds provided detection of swimming reversals with 67 ms resolution, permitting measurement of distinct phases of the responses to attractant and repellent stimuli. After stimulation, there was a latency period in which the population reversal frequency was unchanged, followed by an excitation phase in which reversal frequency increased, and a slower adaptation phase in which reversal frequency returned to its prestimulus value. A step-decrease in illumination of the attractant receptor slow-cycling or sensory rhodopsin (SR) (λ_{max}, 587 nm) was interpreted by the cells as an unfavorable stimulus and, after a minimum latency of 0.70 ± 0.14 s, induced swimming reversals with the peak response occurring 1.34 ± 0.07 s after onset of the stimulus. Two distinct repellent responses in the near UV/blue were observed. (*a*) One was a reversal response to 400 nm light, which was dependent on orange–red background illumination as expected for the photointermediate repellent form of SR (λ_{max}, 373 nm). The minimum latency of this response was approximately the same as that of the SR attractant system. (*b*) The second was a reversal response with shorter minimum latency (0.40 ± 0.07 s) to light of longer wavelength (450 nm) than absorbed by the known SR repellent form. This result confirms recent findings of an additional repellent photosystem in this spectral range. Further, the longer wavelength repellent response is independent of orange–red background illumination, indicating that the photoreceptor mediating this response is not a photointermediate of SR.

INTRODUCTION

Flagellated bacteria exhibit motility responses to a variety of environmental stimuli. Most species are chemotactic, and some are also phototactic, responding to gradients of light intensity. The transient responses of bacteria after environmental changes indicate the operation of two control systems in the taxis machinery. First, upon stimulation of specialized chemoreceptors or photoreceptors in the cell membrane, an excitation system rapidly alters the swimming behavior. Second, an adaptation system returns the cell to its prestimulus behavior (for reviews, see references 1–3).

The molecular events responsible for excitation are obscure, partly due to the difficulty of measuring excitation signal processing times (response latencies). Macnab and Koshland (4) in rapid mixing experiments determined that excitation occurs in unresolved subsecond times for chemotaxis stimuli in *Salmonella typhimurium*. Using iontophoretic stimulation of tethered *Escherichia coli*, Segall, Manson, and Berg (5) measured mean latencies of 0.20 s for individual rotating cells. To study the excitation process, it would be useful to monitor the motility of hundreds of cells with high time resolution after receptor activation. The phototaxis responses of *Halobacterium halobium* provide a way to do this since large numbers of cells can be simultaneously stimulated with temporal precision, and recent developments in computerized cell tracking permit quantitative, time-resolved measurements of the swimming behavior of cell populations. Automated tracking of *H. halobium* at 0.5–1 s resolution using computer-linked systems has been described earlier (6, 7). Here we have coupled an electronic shutter to a commercially-available motion analysis system to extend our time-resolution of swimming behavior to 67 ms.

H. halobium cells exhibit transiently altered swimming reversal probabilities in response to temporal changes in light intensity. Increases of orange–red light and decreases of near-UV/blue light act as favorable stimuli and suppress reversal probabilities, while decreases of orange–red light and increases of near-UV/blue light induce reversals of swimming direction. Genetic, photochemical, and behavioral evidence (7–12) demonstrates that the attractant (orange–red light) receptor is a retinal-containing protein, sensory rhodopsin (SR) (λ_{max}, 587 nm), and that a thermally metastable intermediate (λ_{max}, 373 nm) of the SR photochemical reaction cycle mediates repellent responses in the near-UV. Recently an additional photosystem for repellent taxis has been detected by Takahashi et al. (13) by flash photolysis and action spectra, which show repellent sensitivity in the blue independent of the known

photochemical states of SR. Independently, Wolff et al. (14) have detected a similar repellent sensitivity in the blue by population action spectra.

METHODS

H. halobium strain Flx15 is a $BR^-HR^-SR^+$ (BR, bacteriorhodopsin; HR, halorhodopsin; SR, sensory rhodopsin) mutant isolated by the ion-flux mutant selection procedure (8). Flx15 was chosen for its excellent motility and its BR^-HR^- phenotype. Cells were grown aerobically in peptone medium (8), at 37°C in the dark.

Behavioral Observations

Cells from late exponential phase cultures were diluted 100- to 200-fold in fresh growth medium and incubated for 1–2 h before use in behavioral experiments. The cells were maintained at ~37°C by means of a water-jacketed slide holder on the microscope stage, observed in dark-field with infrared light ($\lambda > 700$ nm) provided by a 12-V, 100-W tungsten-halogen lamp and infrared transmittance filters (7-69; Corning Glass Works, Corning, NY), and detected with an infrared-sensitive video camera (Newvicon; 1 in.; RCA New Products Div., Lancaster, PA) mounted on the microscope. Light stimuli were provided by 150-W Xenon arc lamps, or by a 200-W Mercury arc lamp, the beams from which were combined with the monitoring beam using a cold (visible-reflecting, infrared-transmitting) mirror and beamsplitter (Edmund Scientific Co., Barrington, NJ) before entering the microscope optics. A 600 ± 20 nm interference filter was used for exciting the attractant photosystem, a 520 nm short-pass, 400 ± 5 nm, or 450 ± 20 nm interference filter was used for exciting the repellent photosystems (all from Ditric Optics, Inc., Hudson, MA). Delivery of light stimuli was controlled by means of an electronic shutter (Vincent Associates, Rochester, NY) coupled to the digitizing unit of the automated tracking system (Motion Analysis Corp., Santa Rosa, CA) via a pulse generator (Grass Instrument Co., Quincy, MA) that controlled the delay between an event marker used to initiate data acquisition by the computer and delivery of the stimulus.

Dark-field light intensities were estimated using a photodiode (S1226-8BQ; Hamamatsu Corp., Middlesex, NJ) mounted at the focal plane and calibrated against bright-field intensities measured with a radiometer (Kettering Model 68; Scientific Instruments, Inc., West Palm Beach, FL). Because of difficulties in measuring absolute intensities in dark-field, these values should be considered approximate. Dark-field intensities reported in reference 7 were based on a different method, which greatly underestimated actual values. Intensities were varied by means of neutral density filters (Ditric Optics).

Analysis of Behavioral Data

Automated tracking of swimming *H. halobium* and measurement of light-induced behavioral responses using a computer-linked system has been described earlier by Takahashi and Kobatake (6). Here, we have made use of a commercially available system recently introduced by Motion Analysis Corp. (MAC).

All of the analysis has been carried out using appropriate combinations of the operators defined in the MAC software package. The first stage of analysis is the reduction of video data to generate two-dimensional projections of the cells' swimming paths. Video images are digitized frame-by-frame and transferred to the computer, where a combination of searching operations tracks cells from one frame to the next. The digitizing and search operations require input in the form of user-specified parameters such as frame rate, time interval, and search mask sizes, all of which have been incorporated into a user program, which allows one to automate the process. The version of the program used here digitizes 5-s segments of video data at 15 frames/s, which gives us a maximum time resolution of 67 ms. The program is set up to carry out path calculations on 40 segments of digitized data, followed by merging of the individual path files to form a single file containing information on hundreds of paths.

Examples of paths generated by the program are shown in Fig. 1. The second stage of the analysis makes use of motility parameter calculations to determine if and when reversals occur in a given path, followed by an ensemble summation over the entire collection of paths to determine the total number of reversals occurring at each time point. Here we are using two parameters to identify reversals: the rate-of-change-of-direction (RCDI), which reaches a maximum value when a cell undergoes reversal, and the swimming speed, which passes through a minimum value during reversal. The basic strategy is as follows. RCDI values are calculated for each point along each path, as illustrated in Fig. 2 *A*, followed by application of interval-delta and local-maximum operators to convert the RCDI functions to binary functions. The interval-delta operator is used to set a threshold that distinguishes between RCDI values corresponding to reversals and background fluctuations. The result, as shown in Fig. 2 *C*, is a step-function having a value of unity wherever the RCDI value is above threshold. Similarly, the local-maximum operator picks out each maximum value in the RCDI plot, generating the spike-function shown in Fig. 2 *B*. Multiplying the local-maximum and interval-delta functions together generates a function that has a value of unity wherever the original RCDI function had a maximum value above threshold (Fig. 2 *D*). A similar operation is carried out on the swimming speed function and multiplied with the above to correlate minimum speed with maximum RCDI, our operational definition of reversal. Summing this function over time yields the number of reversals occurring in each path during the analyzed time interval (5 s). The user program is available from the authors.

Response latencies were determined from reversal distributions generated by considering only those paths for which the automated tracking system shows a single reversal, which correlated closely with reversals observed by visual tracking (discussed below). After an ensemble summation of the number of reversals occurring at each frame, the reversal distribution is plotted as a function of time (Fig. 3, *A* and *C*). Delivery of light stimuli was precisely controlled by means of an electronic shutter triggered 1 s after the event marker which initiates the data collection process. Minimum latency times are reported as the first point after

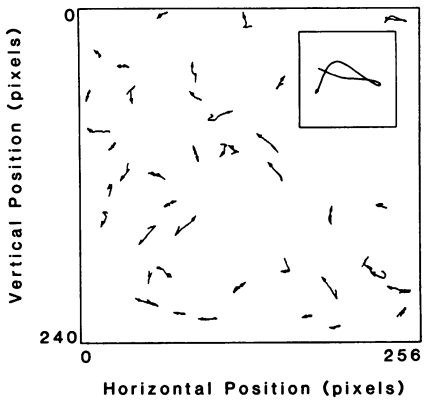

FIGURE 1 Example of paths generated by the motion analysis system. The paths were computed from digitized video images of *H. halobium* mutant Flx15. A series of search operations identifies the number of cells in each video frame, calculates a center-of-mass (centroid) for each object, and tracks the centroids from one frame to the next, thereby generating two-dimensional projections of the cell's swimming trajectories. The paths have been smoothed to minimize small variations in the positions of centroids resulting from the slow translational motion of the cells relative to fluctuations of their digitized outlines. Data was collected at 37°C for 5 s, and processed at 15 video frames per second. A repellent stimulus was delivered 1 s after initiation of data collection. *Inset*, enlarged view of a single path.

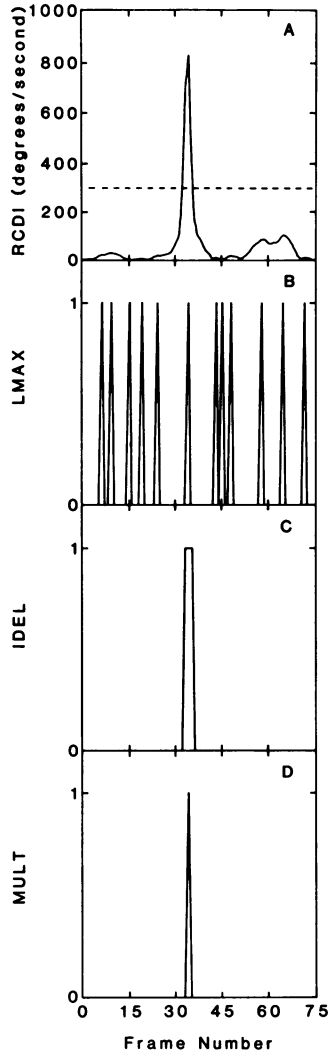

FIGURE 2 Illustration of the strategy used to identify if and when a reversal of swimming direction occurs in a given path. The analysis makes use of appropriate combinations of the operators defined by the MAC software to detect abrupt changes of swimming direction. (*A*) The rate-of-change-of-direction (RCDI) function calculated for the path shown in the inset of Fig. 1. The dotted line indicates a threshold used to discriminate between values of the RCDI function representing reversals from background fluctuations. (*B*) Binary function resulting from application of the local-maximum operator (LMAX) to the RCDI function. (*C*) Binary function resulting from application of the interval-delta operator (IDEL) to the RCDI function using the threshold shown in (*A*). (*D*) Multiplication of (*B*) and (*C*) results in a function having a single spike wherever the original RCDI had a maximum value above threshold. A similar treatment of the swimming speed function is carried out and used to correlate maximum rate-of-change-of-direction with minimum velocity.

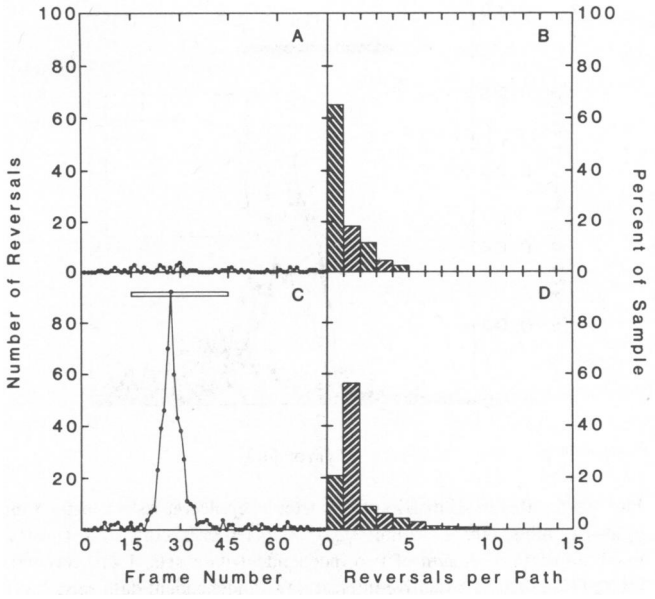

FIGURE 3 Reversal distributions and corresponding histograms of the number of reversals per path. (*A*) Nonstimulated cells. The reversal distribution was obtained by considering paths that showed a single reversal; 306 paths total, 54 with one reversal. The total number of reversals occuring in each frame is determined by ensemble summation. (*B*) Histogram corresponding to data shown in *A;* 21% reversal. Visual tracking of individual cells indicated that, for Flx15, paths showing two or more reversals in a 5-s period were most often the result of out-of-focus cells, immotile cells, and occasional tracking errors. As a measure of response, we use the ratio of the number of paths showing one reversal to the total number showing zero or one reversal. The net tracking efficiency is 80–90%. (*C*) Stimulated cells. A repellent light was turned on 1 s after initiation of data collection. The bar indicates the duration of the stimulus. 974 paths total, 548 with one reversal. (*D*) Histogram corresponding to data shown in *C;* 73% reversal. Note the population shift from the column representing paths with no reversals to that for paths with one reversal.

delivery of the stimulus at which a response above background could be detected.

Histograms of the number of reversals occurring per path are shown in Fig. 3, *B* and *D*. Comparison of visual tracking of individual cells to that done by computer indicated that for strain Flx15, paths showing two or more reversals within the 5-s period were caused by immotile cells, out-of-focus cells, and occasional tracking errors. The program was reasonably efficient in correctly identifying actual reversals (83% of those detected visually) and paths containing no reversals (92% of those detected visually). As a result of the cells' slow translational motion and fluctuating digitized outline, the analysis occasionally gave rise to false reversals. This problem was minimized by smoothing the paths a number of times. The paths shown in Fig. 1 have been smoothed nine times over a window of five frames. The 67-ms time-resolution and the overall tracking efficiency of 80–90% represent improvements over an earlier version of the program (7).

RESULTS

Response Latency of Attractant Photosensing

Cells adapted to continuous orange–red light (600 ± 20 nm) respond to a decrease in the light as an unfavorable stimulus and reverse their swimming direction. The reversal frequency of a population of cells was monitored during such step-down attractant light stimuli delivered at $t = 1$ s in Fig. 4. There is a clearly resolved latency period after stimulation in which the population reversal frequency is unchanged from its prestimulus value, followed by an increase in reversal frequency (excitation) and subsequent return to its prestimulus value (adaptation). For the largest

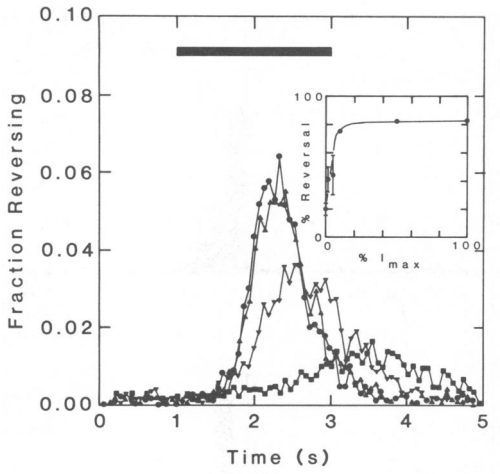

FIGURE 4 Reversal distributions after step-decreases in attractant light. Stimulus, 600 ± 20 nm; I_{max}, 7.8 × 10^4 ergs/cm^2 per s. *Circles,* maximum intensity; sum of two independent data sets; 1,410 reversals total. *Triangles,* 50% relative intensity; two independent data sets; 1,437 reversals total. *Inverted triangles,* 10% relative intensity; two independent data sets; 1,520 reversals total. *Squares,* 5% relative intensity; three independent data sets; 1,294 reversals total. The curves have been normalized to sample size and fraction of cells reversing. The bar indicates the duration of the stimulus. Data was collected for 40 5-s video segments at 30-s intervals. The resulting path files were then merged to form a data set. *Inset,* dose-response curve derived from the data shown in the main figure.

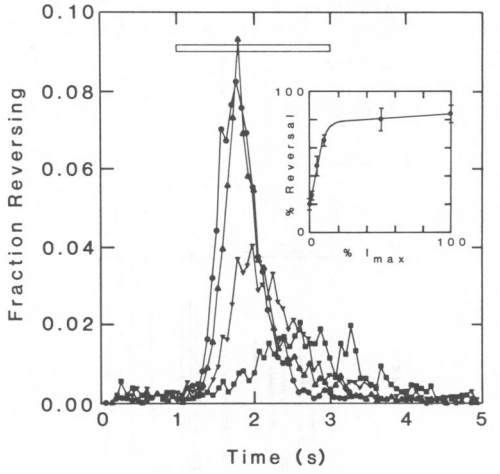

FIGURE 5 Reversal distributions after step-increases in repellent light. Stimulus, 520 nm short-pass; I_{max}, 3.9 × 10^5 ergs/cm^2 per s. *Circles,* maximum intensity; three independent data sets; 2,000 reversals total. *Triangles,* 50% relative intensity; two independent data sets; 1,327 reversals total. *Inverted triangles,* 10% relative intensity; two independent data sets; 1,155 reversals total. *Squares,* 5% relative intensity; two independent data sets; 497 reversals total. The curves have been normalized to sample size and fraction of cells reversing. The bar indicates the duration of the stimulus. *Inset,* dose-response curve derived from the data shown in the main figure.

stimulus in Fig. 4 (circles), the minimum latency period was 0.70 ± 0.14 s (mean ± standard deviation for independent experiments), with the maximum reversal frequency occurring after 1.34 ± 0.07 s. The remaining curves indicate reversal distributions for stimuli of decreasing relative intensity. The distributions are broadened and shifted toward later times, with approximately the same minimum latency (earliest detectable increase over background, ~0.7 s). The maximum light intensity used (7.8 × 10^4 ergs/cm^2 per s) was sufficient to saturate the response (inset). The fraction of cells reversing in the 5-s period saturates with a similar stimulus-dependence as the time to peak reversal frequency.

Response Latencies of Repellent Photosensing

Reversal distributions after step-increases in repellent light (effective bandpass: 360–520 nm; I_{max}, 3.9 × 10^5 ergs/cm^2 per s) are shown in Fig. 5. The distributions are sharper, with a minimum latency of 0.31 ± 0.10 s and a peak at 0.76 ± 0.14 s for the most intense stimulus (circles). Again, lowering the stimulus intensity resulted in broadened, shifted distributions. As with attractant light, repellent light stimuli generate a family of distributions with mean latency decreasing with increasing stimulus strength and with a characteristic minimum latency. The family of distributions characterizing the broad-band repellent response differs from that of the attractant response both in terms of the apparent minimum latency and in the relationship between mean latency and fraction of population undergoing stimulus-induced reversals.

Discrimination of Two Distinct Repellent Photosystems

Previously, it has been reported that repellent sensitivity at ~400 nm is dependent on the presence of red background illumination (10, 11), as expected from the proposal that a blue-absorbing intermediate of the SR molecule acts as a repellent receptor (10). The 520-nm shortpass filter used in the experiments described above was chosen because it delivers a broad-band light, which overlaps the absorption spectra of both the SR ground-state (SR_{587}) and its blue-absorbing photointermediate, S_{373}. In view of a recent report (13) describing an additional repellent sensitivity at longer wavelengths than absorbed by S_{373}, we examined the repellent-stimulus latency using more sharply defined narrow-band filters.

Fig. 6 shows the reversal distributions generated by delivering 400 nm light stimuli in the presence and absence of orange–red background light (600 ± 20 nm). There was a clear increase in the response in the presence of the background light, with a minimum latency of 0.70 ± 0.14 s.

The response to 450 nm light is shown in Fig 7. There is a peak in reversal frequency at ~0.84 s, with a minimum latency of 0.40 ± 0.07 s. Unlike the 400-nm stimulus, the response showed little or no dependence on red background illumination.

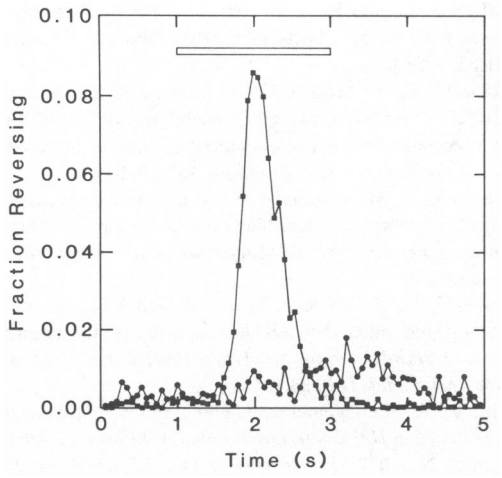

FIGURE 6 Reversal distributions after a step-increase in 400 nm light. Stimulus, 400 ± 5 nm light; I_{max}, 4.0×10^4 ergs/cm^2 per s. *Circles,* infrared background illumination ($\lambda > 700$ nm; 2.8×10^5 ergs/cm^2 per s); two independent data sets; 570 reversals total; 41% reversing within the 5 s period. *Squares,* infrared plus orange–red (600 ± 20 nm; 4.9×10^4 ergs/cm^2 per s) background illumination; two independent data sets; 1,499 reversals total; 83% reversing; minimum latency, ~0.70 ± 0.14 s. The curves have been normalized to sample size and fraction reversing. The bar indicates the duration of the stimulus.

DISCUSSION

We have measured excitation signal processing times in the phototaxis system of *H. halobium.* Swimming behavior was monitored with the use of a commercial digitizer-based motion analysis system coupled to an electronic shutter controlling delivery of light stimuli. Automated analysis of rates of change of direction and linear speeds provided detection of swimming reversals with 67-ms resolution, permitting measurement of both the rapid excitation phase and slower adaptation phase of responses to attractant and repellent photostimuli. The peak response latencies reported here are comparable to the mean latencies of 1–2 s for saturating stimuli measured by visual tracking, and increase with decreasing stimulus strength (15–17). The timescale of the peak response, 0.76–1.34 s, is slower than the 0.20-s mean latency for chemotaxis signalling in *E. coli* measured by Segall *et al.* (5). The slower responses in *H. halobium* may be influenced by signal-generation steps corresponding to the slow photochemical reactions of the receptor molecules. Work is currently in progress to investigate the relationship between behavioral response kinetics and receptor photocycle kinetics.

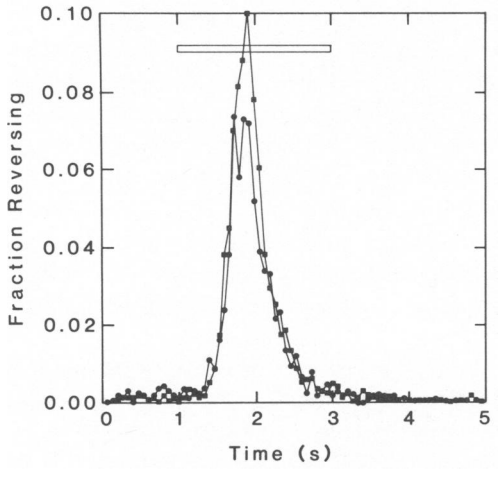

FIGURE 7 Reversal distributions after a step-increase in 450 nm light. Stimulus, 450 ± 20 nm; I_{max}, 3.5×10^5 ergs/cm^2 per s. *Circles,* infrared background illumination (as described for Fig. 6); two independent data sets; 1,164 reversals total; 72% reversal; minimum latency, ~0.40 ± 0.07 s. *Squares,* infrared plus orange–red background illumination (as described for Fig 6); two independent data sets; 1,425 reversals total; 82% reversals. The curves have been normalized to sample size fraction reversing. The bar indicates the duration of the stimulus.

The reversal distributions induced by step-decreases in 600 nm light and step-increases in 400 nm light had approximately the same minimum latency of 0.70 s but different peak times. Reversal induction at these wavelengths and the orange–red light-dependence of the 400-nm response are expected from the properties of the SR attractant form (λ_{max}, 587 nm) and its repellent photointermediate S_{373} (λ_{max}, 373 nm) (9, 10).

Takahashi et al. (13) have recently observed repellent photosensing with peak sensitivity between 450 and 520 nm in a mutant strain (Flx3–12) closely related to Flx15, and report the detection of a flash-induced absorbance change in this region that has different kinetics from that due to SR photocycling. They have suggested that a retinal pigment other than SR mediates this repellent response. The results presented here support this conclusion. The response to 450 nm light is independent of orange–red background illumination, which indicates that the receptor mediating this response is not an SR photointermediate.

The presence of two distinct repellent responses in strain Flx15 indicates that these repellent photosystems can co-exist in the same cells. The reversal distribution after a step-increase in 450 nm light differed from that for the 400 nm light in that the apparent minimum latency was shorter, ~0.40 s compared with 0.70 s for the SR-mediated responses. This may reflect a difference in receptor kinetics, number of receptor molecules required to cycle in order to produce a reversal, or a different manner of integration into the transduction pathway.

We would like to acknowledge the valuable technical assistance and support of L. Amici, D. Cherbavaz, and Dr. W. Hand of Motion Analysis Corp. Dr. Alam greatly acknowledges the generous support and helpful discussions of Dieter Oesterhelt and Gerald Hazelbauer.

This work was supported by Damon Runyon–Walter Winchell Fellowship DRG-839 (Dr. Sundberg), National Institutes of Health grant GM29963, and National Science Foundation (NSF) grant DMB-8416274 (to G. L. Hazelbauer), National Insitutes of Health grants GM27750 and GM34283 (Dr. Spudich), an Irma T. Hirschl Trust Career Scientist Award (Dr. Spudich), and grant DMB-8416123 from the NSF Biological Instrumentation Program (Dr. Spudich).

Received for publication 26 March 1986 and in final form 25 June 1986.

REFERENCES

1. Adler, J. 1975. Chemotaxis in bacteria. *Annu. Rev. Biochem.* 44:341–356.
2. Koshland, D. E., Jr. 1981. Biochemistry of sensing and adaptation in a simple bacterial system. *Annu. Rev. Biochem.* 50:765–782.
3. Berg, H. C. 1983. Random Walks in Biology. Princeton University Press, Princeton, NJ. 1–142.
4. Macnab, R. M. and D. E. Koshland. 1972. The gradient-sensing mechanism in bacterial chemotaxis. *Proc. Natl. Acad. Sci. USA.* 69:2509–2512.
5. Segall, J. E., M. D. Manson, and H. C. Berg. 1982. Signal processing times in bacterial chemotaxis. *Nature (Lond.).* 296:855–857.
6. Takahashi, T., and Y. Kobatake. 1982. Computer-linked automated method for measurement of the reversal frequency in phototaxis of *Halobacterium halobium. Cell Struct. Funct.* 7:183–192.
7. Sundberg, S. A., R. A. Bogomolni, and J. L. Spudich, 1985. Selection and properties of phototaxis-deficient mutants of *Halobacterium halobium. J. Bacteriol.* 164:282–287.
8. Spudich, E. N., and J. L. Spudich. 1982. Control of transmembrane ion fluxes to select halorhodopsin-deficient and other energy-transduction mutants of *Halobacterium halobium. Proc. Natl. Acad. Sci. USA.* 79:4308–4312.
9. Bogomolni, R. A., and J. L. Spudich. 1982. Identification of a third rhodopsin-like pigment in phototactic *Halobacterium halobium. Proc. Natl. Acad. Sci. USA.* 79:6250–6254.
10. Spudich, J. L., and R. A. Bogomolni. 1984. Mechanism of colour discrimination by a bacterial sensory rhodopsin. *Nature (Lond.).* 312:509–513.
11. Takahashi, T., Y. Mochizuki, N. Kamo, and Y. Kobatake. 1985. Evidence that the long-lifetime photointermediate of S-rhodopsin is a receptor for negative phototaxis in *Halobacterium halobium. Biochem. Biophys. Res. Commun.* 127:99–105.
12. Takahashi, T., M. Watanabe, N. Kamo, and Y. Kobatake. 1985. Negative phototaxis from blue light and the role of third rhodopsinlike pigment in *Halobacterium cutirubrum. Biophys. J.* 48:235–240.
13. Takahashi, T., H. Tomioka, N. Kamo, and Y. Kobatake. 1985. A photosystem other than PS370 also mediates the negative phototaxis of *Halobacterium halobium. FEMS (Fed. Eur. Microbiol. Soc.) Microbiol. Lett.* 28:161–164.
14. Wolff, E., R. A. Bogomolni, B. Hess, and W. Stoeckenius. 1986. Phototaxis in *Halobacterium halobium. Biophys. J.* 49:482*a*.
15. Dencher, N. 1978. *In Energetics and Structure of Halophilic Microorganisms.* S. R. Caplan and M. Ginzburg, editors. Elsevier/North Holland, Amsterdam. 67–88.
16. Dencher, N., and E. Hildebrand. 1979. Sensory transduction in *Halobacterium halobium*: Retinal protein pigment controls UV-induced behavioral response. *Z. Naturforsch.* 34:841–847.
17. Schimz, A., and E. Hildebrand. 1985. Response regulation and sensory transduction in *Halobacterium halobium* based on an oscillator. *Nature (Lond.).* 317:641–643.